Nanoscale

PAPER

View Article Online
View Journal | View Issue

Cite this: *Nanoscale*, 2025, **17**, 14827

Electronic structure tunability of carbon-based 1D-polymers combining cross-conjugation and nitrogen doping†

Adriana E. Candia, *[a,b,c] Manuel Vilas-Varela, [d] Myriam H. Aguirre, [e,f] Celia Rogero, [b] David Serrate, [a,e,f] Diego Peña *[d,g] and Jorge Lobo-Checa *[e,f]

Quasi-one-dimensional polymer structures with extended π-electron systems stand out due to their remarkable application in light-emitting diodes and devices. Upon smart choice of their building units, such carbon-based organic nanoarchitectures provide excellent optoelectronic properties by tuning their dimensionality, atomic structure or intrinsic doping. Here, we generate and study three canonical cross-conjugated quasi one-dimensional chains with controlled nitrogen intrinsic doping, which is selectively introduced into their poly-phenylene backbones. By means of scanning tunneling microscopy and spectroscopy we corroborate that the cross-conjugation that break the chain linearity is exclusively responsible of the electronic confinement in the straight segments. Moreover, we demonstrate that the LUMO state exhibits similar spatial distribution for the cross-conjugated polymers independently of the pyridine content of the initial precursor. Despite this coincidence, the semiconducting character and other relevant electronic properties of the polymers are found to depend both on the chain morphology and on the precise position and number of doping nitrogen atoms synthetically introduced into the molecular precursors. We compare these results to related previous studies, which allows us to unambiguously validate the opto-electronic tunability upon the choice of the polymers' building units.

Received 25th March 2025,
Accepted 23rd May 2025

DOI: 10.1039/d5nr01235j

rsc.li/nanoscale

Introduction

Carbon-based organic nanoarchitectures have gained scientific relevance due to the precise control of their electronic, optical, and magnetic properties at the atomic level.[1–5] This versatility position them as promising candidates for low-dimensional material applications[6–12] featuring sophisticated functions such as spintronics,[13–16] gas and energy storage,[17,18] or catalysis and nanoelectronics.[19–23] These advanced functional nanomaterials demand precise synthesis protocols to generate atomically-defined structures presenting controllable physicochemical properties. In this context, on-surface synthesis (OSS) has proven to be an effective strategy for achieving meticulous control over the reaction products and coupling pathways, justifying its implementation in prospective devices.[24] Indeed, OSS has produced countless carbon nanostructures, ranging from graphene nanoribbons with variable widths and edges,[25–36] covalent nanoporous architectures,[37–43] or heteroatom substituted carbon structures.[44–47] From these, the most common OSS reaction is the Ullmann coupling due to its ability to form directional covalent bonds generating zero- to two-dimensional structures in a controlled manner.[24,48]

Quasi-one-dimensional (quasi-1D) polymer structures with extended π-electron systems stand out due to their remarkable physico-chemical properties. For example, the electroluminescence found in poly(*para*-phenylenevinylene) granted its application on blue light-emitting diodes (LED).[49,50] Such technological use triggered the interest to obtain other semiconducting polymers with similar optoelectronic attributes and simultaneously find structural ways to control their properties.

[a]*Laboratorio de Microscopias Avanzadas (LMA), Universidad de Zaragoza, E-50018 Zaragoza, Spain. E-mail: adriana.candia@santafe-conicet.gov.ar*
[b]*Centro de Física de Materiales (CSIC-UPV/EHU), E-20018 San Sebastián, Spain*
[c]*Instituto de Física del Litoral, Consejo Nacional de Investigaciones Científicas y Técnicas, Universidad Nacional del Litoral (IFIS-Litoral, CONICET-UNL), 3000 Santa Fe, Argentina*
[d]*Centro Singular de Investigación en Química Biolóxica e Materiais Moleculares (CiQUS) and Departamento de Química Orgánica, Universidade de Santiago de Compostela, 15782 Santiago de Compostela, Spain. E-mail: diego.pena@usc.es*
[e]*Instituto de Nanociencia y Materiales de Aragon (INMA), CSIC-Universidad de Zaragoza, E-50018 Zaragoza, Spain. E-mail: jorge.lobo@csic.es*
[f]*Departamento de Fisica de la Materia Condensada, Universidad de Zaragoza, E-50009 Zaragoza, Spain*
[g]*Oportunius, Galician Innovation Agency (GAIN), 15702 Santiago de Compostela, Spain*

†Electronic supplementary information (ESI) available. See DOI: https://doi.org/10.1039/d5nr01235j

Indeed, two structural protocols are commonly envisioned to achieve this: (i) by introducing kinks that break the linearity of the chains (cross-conjugation) and, (ii) by selectively exchanging carbon atoms within the monomer units for structurally similar elements with doping character (like nitrogen or boron atoms).

An exemplary case of such electronic tunability is found in poly(*para*-phenylene) (PPP), which is one of the simplest carbon-based 1D chains consisting in straight units of phenyl rings. Particularly, breaking up the linearity of these chains – *i.e.* introducing a *meta*-ligand periodically – results in cross-conjugation that leads to electronic confinement within the straight segments of the zigzag chains, an overall increase of the band gap at the frontier orbitals and a conspicuous reduction of the electron mobility along them central axis of the polymer compared to its PPP counterpart.[51] Alternatively, nitrogen doping by pyridine substitution of the phenyl rings rigidly shifts the energy bandgap without compromising their charge mobility.[52] Thus, the high electron affinity introduced by the N-doping in these polymers is an extra control ingredient that shifts the band structures of the pure carbon polymers.[53]

In this work, we combine the two mechanisms described above (*viz*. variable N-doping concentration and cross-conjugation) to determine the overall effect on the electronic structure of these quasi-1D chains. Notably, we find that the electronic structures deviate from a simple addition of the standalone cases and observe that these effects depend on the precise position and number of N-doping atoms synthetically introduced into the molecular precursors. This study was possible after successful polymerization of three N-doped 4,4″-dibromo-*meta*-terphenyl (DMTP) derivates using OSS protocols on the substrate of Ag(111) (see Fig. 1). The structural and electronic characterization of these zigzag chains was performed by scanning tunneling microscopy (STM) and spectroscopy (STS) techniques in ultra-hight vacuum (UHV) and cryogenic (4.8 K) conditions (see Experimental section). Importantly, we compare our results to previous studies and find that the combination of nitrogen doping and cross-conjugation can reduce the bandgap of the polymers, thereby enabling to structurally control their overall optoelectronic properties.

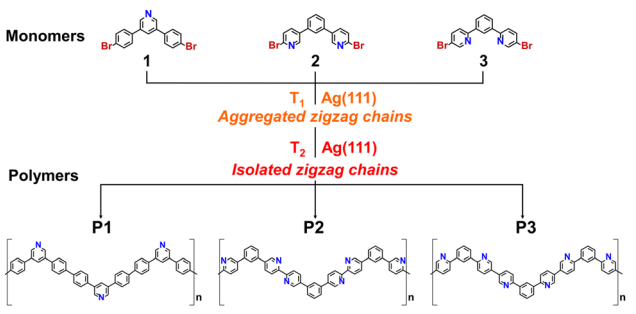

Fig. 1 Scheme of the Ullmann coupling reaction of the three pyridine derivatives of 4,4″-dibromo-*meta*-terphenyl (DMTP) on Ag(111) studied in this work. Hereafter, we will refer to the precursors as **1**, **2** and **3** and to their resulting chain products as **P1**, **P2** and **P3**, respectively. Note the difference in N-atom number and relative positions within precursors and chains.

Results

Structural aspects of the nitrogen-doped covalent zigzag chains

The three aromatic pyridinic precursors (**1**, **2**, and **3**) used in this study are shown in Fig. 1 and differ in the position and number of the nitrogen atoms (refer to the ESI† for details on the synthesis and characterization of these molecular precursors). The halogen atoms occupy *para* positions at the outer rings of the terphenyl derivatives to generate cross-conjugated structures *via* debrominative aryl–aryl coupling on the Ag(111) surface. This substrate was chosen due to the long diffusion lengths sustained by the precursors, which lead to excellent formations of polymeric structures.[51] The room temperature (RT) deposition already leads to partial dehalogenation of some of the precursors, producing intermediate metal–organic products,[54,55] as shown in Fig. S1 of the ESI.† After annealing up to 570 K, long zigzag pyridinic extended covalent chains in a *trans* conformation become the dominant products for the three precursors (see Fig. 2). Notably, these 1D structures merge into large compact islands, where the cleaved chemisorbed Br atoms facilitate this packed arrangement by electrostatically bonding to the peripheral hydrogen atoms of the polymers.[55,56] Statistically, we find that the average inter-chain spacing varies between 1.00 nm and 1.12 nm in the packed islands (similar to previous studies[51]), and the length of the chains extend in average ~25 nm, ~20 nm, and ~15 nm for **P1**, **P2**, and **P3**, respectively (see Fig. S3 and Table S1 of the ESI†).

The middle row panels of Fig. 2 present detailed close-ups of the zigzag polymer chains obtained from the three precursors. The overlaid molecular models agree with quasi-planar geometries of four ring units, where the N atoms of the pyridine groups are expected to reach closer to the substrate and thus appear slightly darker in the images.[52,57] Notably, periodic variations are revealed in the topographic profiles (see Fig. S2 in the ESI†), which match an alternate arrangement of the N atoms within the straight sections of the zigzag chains. This agrees with the configuration obtained from gas phase calculations, that concludes that this arrangement is energetically the most stable due to both the repulsion between neighbouring pyridinic N atoms and the steric hindrance of H atoms at the opposite ends of these rings.[58] Moreover, such alternating nitrogen positioning in adjacent covalently linked pyridines agree with a more efficient proximity conformation to the substrate, following the behavior of other related chains.[57,59–62] Interestingly, the position of these N atoms also influence the packing arrangement, but most importantly, the chain period. Indeed, we statistically find that the periodicity (L) changes from 2.10 nm on **P1**, 2.30 nm for **P2**, and 2.20 nm on **P3** (see Fig. S4 and Table S1 of the ESI†). The origin of such subtle length variation (within ~10%) could be ascribed to

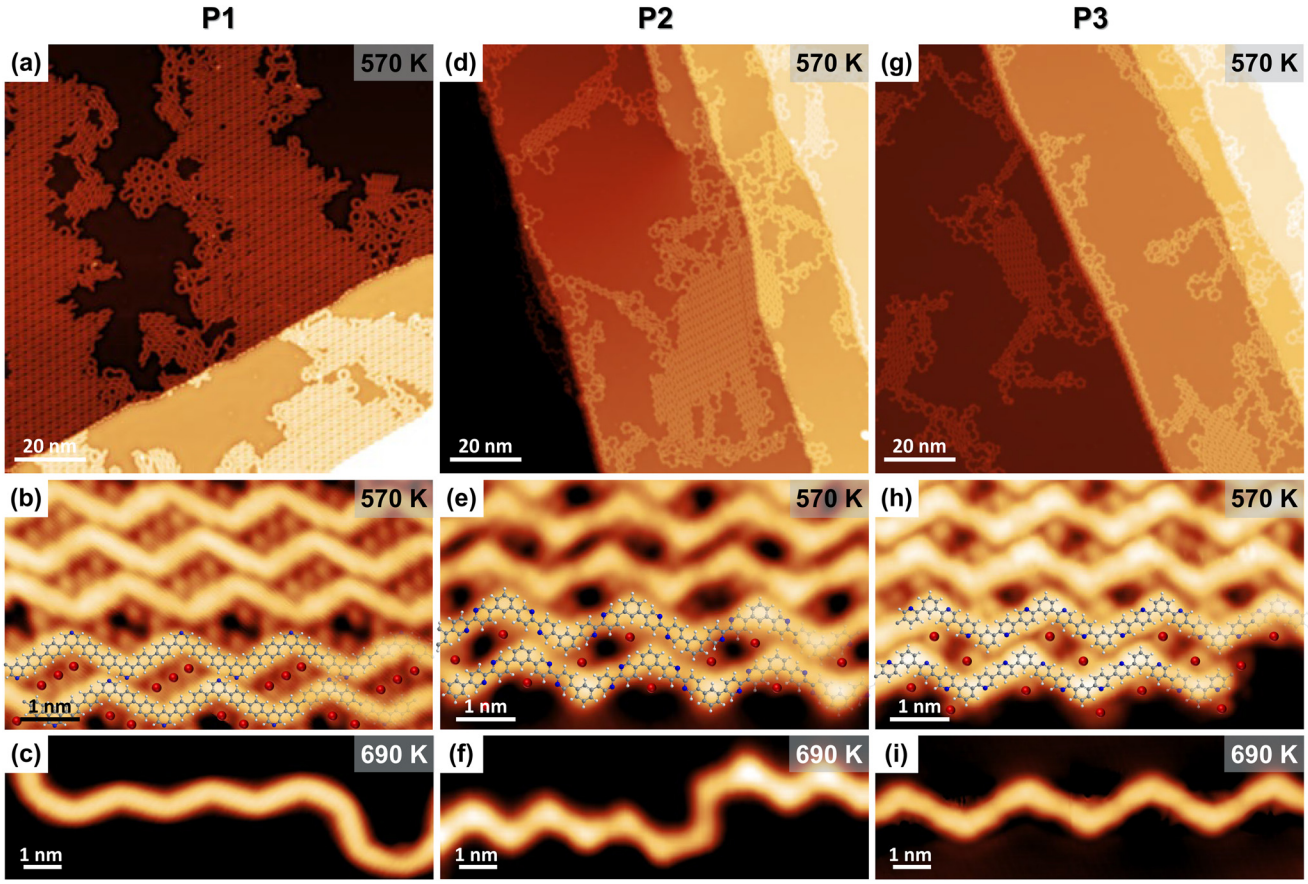

Fig. 2 STM images of the products **P1**, **P2** and **P3**, obtained after OSS of the three precursors on Ag(111) at two different temperatures. The top row images [(a), (d), and (g)] show large-scale views after depositing the precursor at RT and annealing up to 570 K. After reaching this annealing temperature, we find predominance of zigzag polymeric chains aggregated into islands, which mainly follow the three crystallographic directions of the substrate. Images in the middle row [(b), (e), and (h)] are close-ups from the upper row structures that show the detailed morphology of the zigzag chains. Note the parallel alignment of the chains that is partially stabilized by Br adatoms and the overlaid structural models (carbon is represented in gray, hydrogen in white, nitrogen in blue, and bromine in red). The bottom row [(c), (f), and (i)] display high-resolution images of isolated zigzag chains emerging after annealing the systems up to 690 K. Note the darker intensity at the central region of the straight sections in (e), (f), (h) and (i) that coincides with the nitrogen sites (further details in Fig. S2 of the ESI†). STM parameters: (a) I = 80 pA, V = −1.0 V; (b) I = 110 pA, V = −1.5 V; (c) I = 30 pA, V = −0.4 V; (d) I = 50 pA, V = −1.0 V; (e) I = 50 pA, V = −1.0 V; (f) I = 110 pA, V = −0.01 V; (g) I = 100 pA, V = −0.1 V; (h) I = 100 pA, V = −0.1 V; (i) I = 50 pA, V = 0.01 V.

different registries with the substrate (defined by the neighboring nitrogen separation) or to the electronic effects reported in the next section.

The zigzag polymeric structures were annealed up to 690 K (avoiding degradation) to laterally fuse them, as for other related terphenyl-based precursors[57,59] or their straight PPP counterparts.[63] Despite the high temperatures reached, controlled lateral fusion of the zigzag chains was absent in the three cases. At such high temperature annealing, the Br atoms desorb from the surface, so the electrostatic stabilizing role of these by-products between chains is lost and the previous close-packed islands disaggregate. In this way, the chains adopt disordered conformations with a significantly higher number of bends and twists along their length promoted by *cis* linkages that were practically absent previously (see Fig. S5 of the ESI†). Despite this greater structural flexibility, the disordered individual polymeric strands maintain in part their previous zigzag structure (see bottom row of Fig. 2), allowing us to access their electronic structure.

Electronic properties of nitrogen-doped covalent zigzag chains

The absence of lateral fusion and the disaggregation creates the perfect playground to investigate the electronic properties of the isolated cross-conjugated polymers. We do this by scanning tunneling spectroscopy (STS) recording both conductance (dI/dV) line scans and dI/dV grids regulating at constant set points to extract spectroscopy maps. These maps are acquired in constant current mode with the tip–sample distance being defined by the setpoint parameters. Fig. 3 displays on the top row the dI/dV point spectra at the center of a straight section, on the central row the spectral colormaps obtained from line scans along straight sections, and on the bottom row, a representative topography with unoccupied and occupied dI/dV maps of the three types of isolated chains.

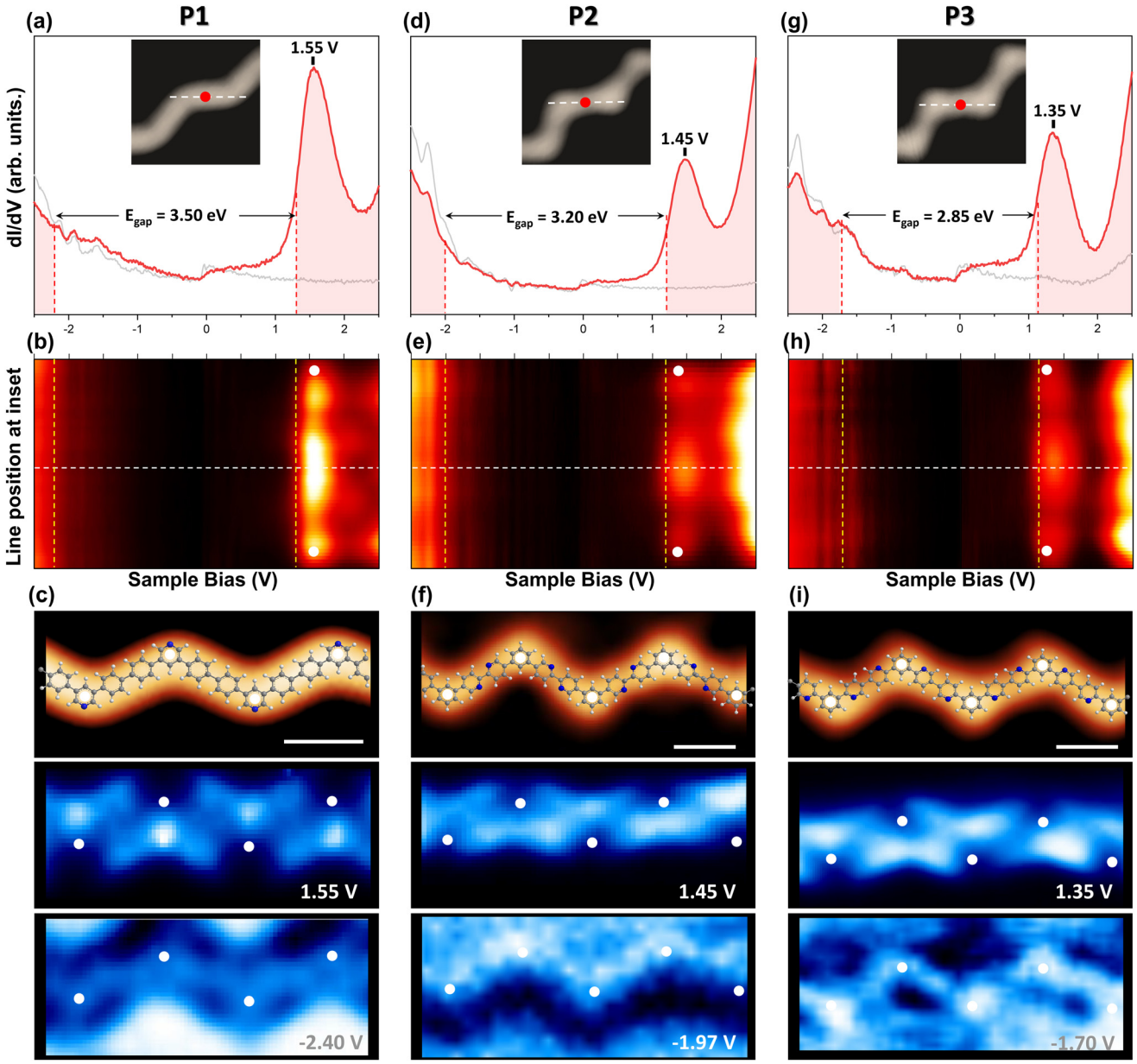

Fig. 3 Electronic structure determination of isolated **P1** (left column), **P2** (central column) and **P3** (right column) on Ag(111). The point spectra, d*I*/d*V* line scans and isoenergetic maps (obtained from d*I*/d*V* grids regulating at constant set points) were recorded from isolated chains after the annealing treatment up to 690 K. The top row panels [(a), (d), (g)] display constant-height d*I*/d*V* point spectra acquired around the center of a straight section, with the Ag(111) STS shown in gray for comparison. The insets show topographic images of the zigzag chains marking the STS position (red dots) and the line scan trajectories for the central panels (white discontinuous lines). The middle row panels [(b), (e), (h)] display line scan colormaps consisting of several d*I*/d*V* spectra acquired at constant-height along the straight section of the chains. The valence band (VB) and conduction band (CB) onsets are indicated by vertical yellow dashed lines and appended as shaded areas at the top row, which define the semiconducting band gaps (quatified in the top panels). Some tip states are present in these colormaps featuring fixed energies with intensity modulation absence. The bottom row panels [(c), (f), (i)] display topographic (top) and d*I*/d*V* maps (bright more intense) at the dominant unoccupied peak energies (LUMO) and close to the VB onset (bottom). These d*I*/d*V* maps (extracted from conductance grids) evidence similar spatial distribution of the LUMO states in the three cases (white circles guide the eye marking the corner ring centers). STM parameters: (a) I = 20 pA, V = −0.5 V; (d) I = 10 pA, V = −0.4 V; (g) I = 30 pA, V = −0.4 V; (c) I = 15 pA, V = −0.5 V; (f) I = 10 pA, V = −0.4 V; (i) I = 30 pA, V = −0.4 V. STS parameters: bias voltage modulation of 15 mV_{rms} at 817.3 Hz with the following setpoints: (a–c) V = −0.4 V, I = 20 pA; (d–f) V = −0.4 V, I = 10 pA and (g–i) V = −0.8 V, I = 50 pA. Inset scales: 1 nm.

In the unoccupied region ($V > 0$ polarization range) shown in the top and middle rows of Fig. 3, dominant peaks are observed at 1.55 V, 1.45 V, and 1.35 V for the **P1**, **P2** and **P3** chains, respectively. The spatial distribution at these energies (central row of Fig. 3c) is similar to the one found in the undoped zigzag polyphenylene chain at an energy of 1.9 V

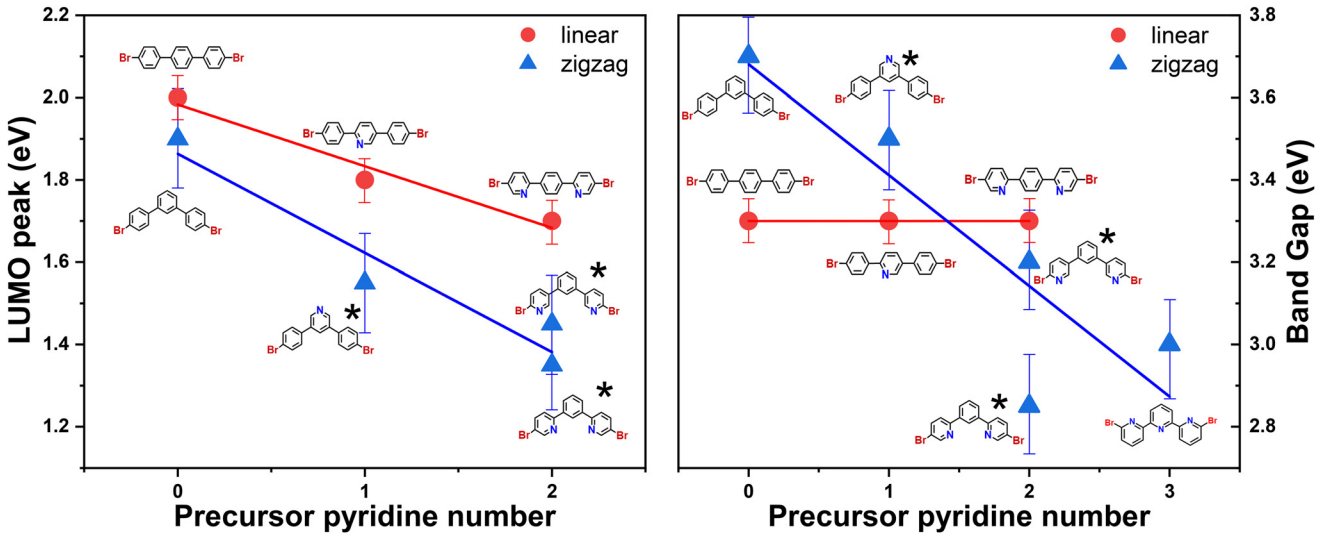

Fig. 4 Comparison of the LUMO energy positions (left graph) and band gaps (right graph) of linear and zigzag polymeric chains as a function of the pyridine groups contained in the precursors. Here, the pyridine number is proportional to the fraction of nitrogen heteroatoms of 1D extended conjugated polymer systems.[52,64,65] The red circles correspond to the linear chains, while the blue triangles relate to zigzag chains. Each point is accompanied by its precursor molecule,[51,52,59] highlighting with asterisks the molecules used in this work. Color coded linear fits are added to help visualizing the effects. The error bars introduce a 5% margin to all presented values to account for possible experimental uncertainties. Further details can be found in Table S2 and the ESI.†

(imaged in constant-height with a CO-functionalized tip). Considering the different experimental acquisition conditions between them, this state is identified as the lowest unoccupied molecular orbital (LUMO) state.[51] Interestingly, we find that the pyridine-doped chains exhibit a progressive energy decrease of these LUMO peaks with increasing content of N atoms in the unit cell (see Fig. 4). However, we observe that the precise structural position of the N atoms at the straight segments do also affect the final energy position of these peaks (compare the **P2** and **P3** chains in Fig. 3 and 4).

Line scans along the straight sections of the undoped zigzag polyphenylene chain allowed to visualize the LDOS distribution of this LUMO state.[51] It was identified as the first stationary state of a particle in a box (n = 1) that was localized in the straight segments of the zigzag structure. Notably, we find in the **P1**, **P2** and **P3** chains a similar intensity distribution with maxima at the center and extinction at the cross-conjugated elbows (see central row of Fig. 3). This evidences a very similar electronic character of the N-doped chains and the undoped zigzag polyphenylene chains. We can then conclude that the confining properties come as a consequence of the presence of meta-type junctions that act as scattering barriers for polymer electrons, regardless of atomic conformations and the presence of the pyridine groups.[51,66,67]

Relying in all the extracted electronic structure datasets (Fig. 3 and Fig. S6 of the ESI†), we could determine the onset positions of both the valence bands (VB) and the conduction bands (CB), which define the semiconductive gaps of these chains. In all datasets the onset of the CB was conspicuous and is indicated by dotted vertical lines in Fig. 3. Contrarily, the VB onsets were highly challenging to define due to a reduced tip–sample stability at large negative bias voltages and a larger contribution of tip states in the occupied region. At such high negative bias, the dI/dV maps exhibit a weak extended highest occupied molecular orbital (HOMO) state mainly following the polymer structure (see bottom of Fig. 3 and Fig. S6 of the ESI†). Intensity inversion or asymmetries can be detected in these conductance maps, which can be attributed to slightly different scanning conditions and to different atomic tip terminations that modify the electronic sensitivity and introduce subtle variations on the electronic visualization. Comparing the substrate contribution from the polymeric chains LDOS in different dI/dV grids, we could approximately set this VB onset energy and extract the energy gaps that amounted to 3.50 eV, 3.20 eV, and 2.85 eV for the **P1**, **P2** and **P3** chains, respectively. Again, we find a dependence on both the number of N atoms and their precise distribution within the unit cell for the experimental band gaps (see Fig. 4).

Discussion

Our results show that these chains do not laterally fuse, even when annealed to considerably high temperatures, which could misleadingly lead to the conclusion that these chains are energetically more stable than other related polymeric chains. Indeed, related terphenyl based precursors with *meta*-positioned halogens (instead of *para*-, like in this work) fuse in two steps, first forming aligned macrocycles and later forming nitrogen-doped porous carbon nanoribbons.[57,59] However, we note that linear chains containing pyridine rings were never reported to laterally fuse, contrarily to their pristine

counterparts.[52,63,68] As nitrogen atoms within pyridines won't covalently bond to an adjacent dehydrogenated carbon it seems way too unfavorable to leave unsaturated bonds within fused structures. Thus, the presence of N-atoms must efficiently hinder that fusion whenever these atoms are necessarily confronted with C–H groups.

Another thing to consider is whether the pyridinic nitrogens could increase the torsional angle between adjacent rings due to its stronger interaction with the substrate. Although we cannot totally discard the modification of the twist angles with respect to the purely unsubstituted phenyl chains, the difference must be subtle because we do not find a relevant alteration in the spatial distribution of the frontier electronic states nor any effective reduction of the π-conjugation with N content in these polymers.[52]

An interesting aspect to be discussed is the comparison of the LUMO positions and the energy gaps with respect to other similar poly-phenylene chains as a function of nitrogen content in the precursor (proportional to the fraction of nitrogen heteroatoms). We limit our comparison to the Au and Ag substrates as the interfacial interactions that could impact the electronic results are minimized. As shown on the left graph of Fig. 4, adding pyridines to the precursor has a downshifting effect on the LUMO, which shifts the energy of this state towards the Fermi level both for linear and zigzag chains. This can be reasoned as an effective intrinsic electronic doping of the resulting polymers. We find that this downshift is practically linear with precursor pyridine number, but it is more pronounced for the zigzag chains. Interestingly, the position occupied by the nitrogen atom influences the doping level, based on the less pronounced downshift variation observed for **P2** with respect to **P3**. This means that the electronic doping is less efficient when the two nitrogens are closests, possibly introducing some sort of Coulomb repulsion. Thus, the system might try to reduce such electronic repulsion by stretching the unit cell, becoming largest for **P2** (see Table S1 of the ESI†).

Regarding the bandgaps (right graph of Fig. 4), we find remarkable differences with the overall chain morphology. For linear chains, the band gap is reported to be unchanged independently of the number of N atoms in the polymer. This means that both frontier orbitals experience a rigid shift towards lower polarization voltages that is caused by the intrinsic doping of the pyridinic groups.[52] Contrarily, the zigzag polymeric chains exhibit a striking decrease of the energy gap with N content. Because the bandgap modification is more significant with N content than the LUMO energy shift, we find that both frontier orbitals move towards the Fermi energy. This behavior difference of the bandgap must be related to the topology of the zigzag chain that can induce electronic confinement in the short straight sections. We infer that such electron localization must in turn increase the sensitivity to the nitrogen incorporation in the backbone (intrinsic dopants). These N atoms produce an electronic perturbation in the form of asymmetric charge redistribution that effectively reduce the energy gap. In contrast, the linear chains allow the electrons to move practically unperturbed along the chain axis, so that structural dopants affect much less the overall electronic properties. Thus, the presence of N heteroatoms leads to a rigid energetic shift of the frontier orbitals. Importantly, this change in the frontier orbitals of the zigzag chains is not only dependent on the pyridine content within the structure, but also upon the exact atomic position occupied within the ring. In this case, the polymeric chain becomes more conductive, when the two nitrogens are farther apart, *i.e.* for **P3** chains. Thus, the type of molecular linkage (*para- vs. meta-*), the nitrogen content (pyridine groups added on the precursors) and the ultimate position of the nitrogen atoms (atomic structure) contribute to the modulation of the electronic character of the polymeric chains. Through selective combination of all these ingredients, we envision the control of both the LUMO position and the bandgap size of these 1D-polymeric chains, with the prospect of tuning their ultimate opto-electronic properties. We hope that this experimental work triggers the interest of research groups to perform theoretical calculations on these polymeric systems, which can shed light into the role of Coulomb repulsion between the doping centers on the band structure.

Conclusions

Combining cross-conjugation and intrinsic nitrogen-doping in zigzag polymeric chains, we demonstrate the tunability of their electronic properties by means of STM/STS. The quasi-1D structures were successfully generated by on-surface synthesis on Ag(111) using three *meta*-terphenyl derivatives. We corroborate that in these extended π-electron systems, the cross-conjugation that breaks the chain linearity is solely responsible for the electronic confinement within the straight sections. Indeed, the LUMO exhibits a common spatial distribution on the polymers independently of the pyridine content within the structure. Contrarily, the exact position and amount of nitrogen atoms incorporated into the precursors are key in defining the overall electronic character of these 1D-polymers, as they influence the LUMO position and bandgap size. This study underscores the importance of molecular design, not only in terms of dopant quantity, but also in their precise location within the structure. Controlling the structural properties to the atomic level is the only way to envision full control of the electronic properties in 1D-conjugated polymers, which might open new avenues for advanced opto-electronic device applications.

Experimental section

The molecular precursors **1**, **2** and **3** were obtained by solution chemistry by means of Pd-catalyzed Suzuki–Miyaura couplings. See the ESI† for details on the preparation and characterization of these molecules. All experiments were performed *in situ* in UHV conditions, with a base pressure in the range of 1×10^{-10} mbar. A silver crystal surface oriented in the (111)

direction was used for the polymer synthesis. The substrate cleaning was carried out by repeated cycles of Ar^+ ion sputtering at energies of 1.0 keV, followed by annealing at 700 K, resulting in clean, ordered surfaces with wide terraces.

The organic structures were prepared in UHV by thermal evaporation from a Knudsen cell at constant temperatures of 358 K, 363 K, and 366 K for the precursors **1**, **2**, and **3**, respectively, at rates of approximately 0.03 monolayers (ML) per minute, while the Ag(111) substrate was kept at room temperature. The precursor coverage was chosen in the range between 0.5 and 0.7 ML. To check the precursor integrity during evaporation, some depositions were done at 150 K, as reported in the ESI.† Room temperature deposition led to partial dehalogenation of the molecules, with both intact (minor proportion) and dissociated molecules observed, as shown in Fig. S1 of the ESI.† This dehalogenation produced intermediate products in which the precursor molecules initially coordinated with mobile Ag adatoms on the surface, forming C–Ag–C metal–organic bonds.[54,55] These deposition were followed by successive annealings up to 570 K and 690 K during 15 minutes.

Low-temperature scanning tunneling microscopy and spectroscopy (LT-STM/STS) investigations were conducted with a Scienta Omicron LT-qplus microscope, cooled down to 4.8 K in a liquid helium bath and controlled by a Matrix SPM system. A tungsten (W) tip was used in all experiments, and all bias voltages are referenced to the sample. LT-STS spectra and maps were obtained through a lock-in amplifier with an oscillation frequency of f_{osc} = 817.3 Hz and a modulation amplitude of V_{RMS} = 10.0–15.5 mV. All images presented were acquired in constant current mode, unless otherwise stated. The analysis of the STM images was performed using the image processing Gwyddion 2.63 software.[69]

Author contributions

A. E. C., J. L.-C. conducted the STM/STS experiments and data analysis with help from D. S.; M. V.-V. and D. P. designed and synthesized the precursors; A. E. C. and J. L.-C. wrote the manuscript and conceived the project; all authors contributed to the discussion and final revision of the manuscript.

Data availability

The data supporting this article have been included as part of the ESI.†

Conflicts of interest

The authors declare no competing interest.

Acknowledgements

We thank Ivan Abadías-Arnal and Leyre Hernández-López for their help in the initial stages of this project. We are also grateful to Carlos Martín-Sacristán for continuous technical support. We further acknowledge the use of Servicio General de Apoyo a la Investigación-SAI and the Laboratorio de Microscopías Avanzadas of the Universidad de Zaragoza for access to the equipments and resources. A. E. C. thanks finanacial support from grant PICT-INVI-00863 of the Consejo Nacional de Investigaciones Científicas y Técnicas (CONICET) and the Agencia Nacional de Promoción Científica y Tecnológica (ANPCyT) and also the financial support through IKUR Strategy under the collaboration agreement between Ikerbasque Foundation and Materials Physics Center on behalf of the Department of Education of the Basque Government. We further acknowledge financial support from Grant References No. PID2022-138750NB-C21 (J. L.-C., A. E. C., D. S.), PID2022-140845OB-C62 (D. P. and M. V.-V.) funded by MCIN/AEI/10.13039/501100011033, by "ERDF A way of making Europe" and "European Union NextGenerationEU/PRTR". Also financing from the European Research Council under European Union's Horizon 2020 research and innovation programme of Marie Skłodowska-Curie grant agreement ULTIMATE-I No 101007825 (M. H. A., A. E. C., J. L.-C.) is acknowledged. We also thank the Aragonese Projects RASMIA E12_23R (J. L.-C.) and NANOMIDAS E13_23R (D. S., M. H. A.), co-funded by Fondo Social Europeo. We thank support from the European Regional Development Fund of the European Union and from Xunta de Galicia (Centro de Investigacion de Galicia accreditation 2019–2022, ED431G 2019/03).

References

1 S. Y. Hong, D. Y. Dim, C. Y. Kim and R. Hoffmann, Origin of the Broken Conjugation in m-Phenylene Linked Conjugated Polymers, *Macromolecules*, 2001, **34**, 6474–6481.
2 T. Markussen, R. Stadler and K. S. Thygesen, The Relation between Structure and Quantum Interference in Single Molecule Junctions, *Nano Lett.*, 2010, **10**, 4260–4265.
3 A. A. Kocherzhenko, F. C. Grozema and L. D. A. Siebbeles, Single Molecule Charge Transport: From a Quantum Mechanical to a Classical Description, *Phys. Chem. Chem. Phys.*, 2011, **13**, 2096–2110.
4 P. A. Limacher and H. P. Lüthi, Cross-Conjugation, *Wiley Interdiscip. Rev.:Comput. Mol. Sci.*, 2011, **1**, 477–486.
5 D. Z. Manrique, C. Huang, M. Baghernejad, X. Zhao, O. Al-Owaedi, H. Sadeghi, V. Kaliginedi, W. Hong, M. Gulcur, T. Wandlowski, M. R. Bryce and C. J. Lambert, A Quantum Circuit Rule for Interference Effects in Single-Molecule Electrical Junctions, *Nat. Commun.*, 2015, **6**, 6389.
6 J. M. Cai, P. Ruffieux, R. Jaafar, M. Bieri, T. Braun, S. Blankenburg, M. Muoth, A. P. Seitsonen, M. Saleh, X. L. Feng, K. Müllen and R. Fasel, Atomically precise

bottom-up fabrication of graphene nanoribbons, *Nature*, 2010, **466**, 470–473.
7 S. Blankenburg, J. M. Cai, P. Ruffieux, R. Jaafar, D. Passerone, X. Feng, K. Müllen, R. Fasel and C. A. Pignedoli, Intraribbon Heterojunction Formation in Ultranarrow Graphene Nanoribbons, *ACS Nano*, 2012, **6**, 2020–2025.
8 Y.-C. Chen, D. G. de Oteyza, Z. Pedramrazi, C. Chen, F. R. Fischer and M. F. Crommie, Tuning the band gap of graphene nanoribbons synthesized from molecular precursors, *ACS Nano*, 2013, **7**, 6123–6128.
9 C. Bronner, S. Stremlau, M. Gille, F. Braußе, A. Haase, S. Hecht and P. Tegeder, Aligning the band gap of graphene nanoribbons by monomer doping, *Angew. Chem., Int. Ed.*, 2013, **52**, 4422–4425.
10 S.-Y. Ding and W. Wang, Covalent organic frameworks (COFs): from design to applications, *Chem. Soc. Rev.*, 2013, **42**, 548–568.
11 J. Sakamoto, J. van Heijstand, O. Lukin and A. D. Schlüter, Two-Dimensional Polymers: Just a Dream of Synthetic Chemists?, *Angew. Chem., Int. Ed.*, 2009, **48**, 1030–1069.
12 J. Colson and W. Dichtel, Rationally Synthesized Two-Dimensional Polymers, *Nat. Chem.*, 2013, **5**, 453–465.
13 M. Bazarnik, B. Bugenhagen, M. Elsebach, E. Sierda, A. Frank, M. H. Prosenc and R. Wiesendanger, Toward Tailored All-Spin Molecular Devices, *Nano Lett.*, 2016, **16**, 577–582.
14 M. Hatanaka, Band structures of porous graphenes., *Chem. Phys. Lett.*, 2010, **488**, 187–192.
15 A. Baskin and P. Král, Electronic structures of porous nanocarbons, *Sci. Rep.*, 2011, **36**, 1.
16 M. Hatanaka, Magnetic Ordering in Porous Graphenes, *J. Phys. Chem. C*, 2012, **116**, 20109–20120.
17 S. Gadipelli and Z. X. Guo, Graphene-based materials: synthesis and gas sorption, storage and separation, *Prog. Mater. Sci.*, 2015, **69**, 1–60.
18 K. P. Loh, S. W. Tong and J. Wu, Graphene and graphene-like molecules: prospects in solar cells, *J. Am. Chem. Soc.*, 2016, **138**, 1095–1102.
19 L. Lafferentz, F. Ample, H. Yu, S. Hecht, C. Joachim and L. Grill, Conductance of a single conjugated polymer as a continuous function of its length, *Science*, 2009, **323**, 1193–1200.
20 H. Wang, H. S. Wang, C. Ma, L. Chen, C. Jiang, C. Chen, X. Xie, A.-P. Li and X. Wang, Graphene nanoribbons for quantum electronics, *Nat. Rev. Phys.*, 2021, **3**, 791–802.
21 P. Xu, J. Yang, K. Wang, Z. Zhou and P. Shen, Porous graphene: Properties, preparation, and potential applications, *Chin. Sci. Bull.*, 2012, **57**, 2948–2955.
22 I. Silveiro, J. M. P. Ortega and F. J. G. de Abajo, Quantum nonlocal effects in individual and interacting graphene nanoribbons, *Light:Sci. Appl.*, 2015, **4**, e241.
23 M. Bieri, M. Treier, J. Cai, K. Aït-Mansour, P. Ruffieux, O. Gröning, P. Gröning, M. Kastler, R. Rieger, X. Feng, K. Müllen and R. Fasel, Porous graphenes: two-dimensional polymer synthesis with atomic precision, *Chem. Commun.*, 2009, **45**, 6919–6921.
24 Q. Shen, H.-Y. Gao and F. Harald, Frontiers of on-surface synthesis: From principles to applications, *Nano Today*, 2017, **13**, 77–96.
25 Y.-C. Chen, D. G. de Oteyza, Z. Pedramrazi, C. Chen, F. R. Fischer and M. F. Crommie, Tuning the band gap of graphene nanoribbons synthesized from molecular precursors, *ACS Nano*, 2013, **7**, 6123–6128.
26 P. Han, K. Akagi, F. F. Canova, H. Mutoh, S. Shiraki, K. Iwaya, P. S. Weiss, N. Asao and T. Hitosugi, Bottom-up graphene-nanoribbon fabrication reveals chiral edges and enantioselectivity, *ACS Nano*, 2014, **8**, 9181–9187.
27 H. Zhang, H. Lin, K. Sun, L. Chen, Y. Zagranyarski, N. Aghdassi, S. Duhm, Q. Li, D. Zhong, Y. Li, K. Müllen, H. Fuchs and L. Chi, On-surface synthesis of rylene-type graphene nanoribbons, *J. Am. Chem. Soc.*, 2015, **137**, 4022–4025.
28 J. Liu, B.-W. Li, Y.-Z. Tan, A. Giannakopoulos, C. Sanchez-Sanchez, D. Beljonne, P. Ruffieux, R. Fasel, X. Feng and K. Müllen, Toward cove-edged low band gap graphene nanoribbons, *J. Am. Chem. Soc.*, 2015, **18**, 6097–6103.
29 S. Kawai, S. Saito, S. Osumi, S. Yamaguchi, A. S. Foster, P. Spijker and E. Meyer, Atomically controlled substitutional boron-doping of graphene nanoribbons, *Nat. Commun.*, 2015, **6**, 8098.
30 P. Ruffieux, S. Wang, B. Yang, C. Sánchez-Sánchez, J. Liu, T. Dienel, L. Talirz, P. Shinde, C. A. Pignedoli, D. Passerone, T. Dumslaff, X. Feng, K. Müllen and R. Fasel, On-surface synthesis of graphene nanoribbons with zigzag edge topology, *Nature*, 2016, **531**, 489–492.
31 L. Talirz, H. Söde, T. Dumslaff, S. Wang, J. R. Sanchez-Valencia, J. Liu, P. Shinde, C. A. Pignedoli, L. Liang, V. Meunier, N. C. Plumb, M. Shi, X. Feng, A. Narita, K. Müllen, R. Fasel and P. Ruffieux, On-surface synthesis and characterization of 9-atom wide armchair graphene nanoribbons, *ACS Nano*, 2017, **11**, 1380–1388.
32 S. Kawai, S. Nakatsuka, T. Hatakeyama, R. Pawlak, T. Meier, J. Tracey, E. Meyer and A. Foster, Multiple heteroatom substitution to graphene nanoribbon, *Sci. Adv.*, 2018, **4**, eaar7181.
33 S. Kewei, J. Penghui, Z. Junjie, W. Jinxi, X. Li, X. Xin, Z. Haiming and C. Lifeng, On-surface synthesis of 8- and 10-armchair graphene nanoribbons, *Small*, 2019, **15**, 1804526.
34 S. Kewei, X. Li, C. Long, Z. Haiming and C. Lifeng, Substrate-Controlled Synthesis of 5-Armchair Graphene Nanoribbons, *J. Phys. Chem. C*, 2020, **124**, 11422–11427.
35 M. Telychko, *et al.*, Ultrahigh-yield on-surface synthesis and assembly of circumcoronene into a chiral electronic kagome-honeycomb lattice, *Sci. Adv.*, 2021, **7**, eabf0269.
36 R. S. K. Houtsma, J. de la Rie and M. Stöhr, Atomically precise graphene nanoribbons: interplay of structural and electronic properties, *Chem. Soc. Rev.*, 2021, **50**, 6541–6568.
37 C. Moreno, M. Vilas-Varela, B. Kretz, A. Garcia-Lekue, M. V. Costache, M. Paradinas, M. Panighel, G. Ceballos,

S. O. Valenzuela, D. Peña and A. Mugarza, Bottom-up synthesis of multifunctional nanoporous graphene, *Science*, 2018, **360**, 199–203.

38 J. Hieulle, *et al.*, On-surface route for producing planar nanographenes with azulene moieties, *Nano Lett.*, 2018, **18**, 418–423.

39 Q. Fan, D. Martin-Jimenez, S. Werner, D. Ebeling, T. Koehler, T. Vollgraff, J. Sundermeyer, W. Hieringer, A. Schirmeisen and J. M. Gottfried, On-Surface Synthesis and Characterization of a Cycloarene: C108 Graphene Ring, *J. Am. Chem. Soc.*, 2020, **142**, 894–899.

40 J. Su, P. Mutombo, X. Peng, S. Song, M. Ondráček, P. Golub, J. B. L. Veis, M. Telychko, P. Jelínek, J. Wu and J. Lu, On-surface synthesis and characterization of [7]triangulene quantum ring, *Nano Lett.*, 2021, **21**, 861–867.

41 X. Zhu, Y. Liu, W. Pu, F.-Z. Liu, Z. Xue, Z. Sun, K. Yan and P. Yu, On-surface synthesis of C144 hexagonal coronoid with zigzag edges, *ACS Nano*, 2022, **16**, 10600–10607.

42 F. Xiang, S. Maisel, S. Beniwal, V. Akhmetov, C. Ruppenstein, M. Devarajulu, A. Dörr, O. Papaianina, A. Görling, K. Y. Amsharov and S. Maier, Planar π-Extended cycloparaphenylenes featuring an allarmchair edge topology, *Nat. Chem.*, 2022, **14**, 871–876.

43 L. Grill, M. Dyer, L. Lafferentz, M. Persson, M. V. Peters and S. Hecht, Nano-architectures by covalent assembly of molecular building blocks, *Nat. Nanotechnol.*, 2007, **2**, 687–691.

44 T. H. Vo, M. Shekhirev, D. A. Kunkel, F. Orange, M.-F. Guinel, A. Enders and A. Sinitskii, Bottom-up solution synthesis of narrow nitrogen-doped graphene nanoribbons, *Chem. Commun.*, 2014, **50**, 4172.

45 X. Wang, *et al.*, Heteroatom-doped perihexacene from a double helicene precursor: on-surface synthesis and properties, *J. Am. Chem. Soc.*, 2017, **139**, 4671–4674.

46 X. Wang, *et al.*, xploration of pyrazine-embedded antiaromatic polycyclic hydrocarbons generated by solution and on-surface azomethine ylide homocoupling, *Nat. Commun.*, 2017, **8**, 1948.

47 I. Piskun, R. Blackwell, J. Jornet-Somoza, F. Zhao, A. Rubio, S. G. Louie and F. R. Fischer, Covalent C–N bond formation through a surface catalyzed thermal cyclodehydrogenation, *J. Am. Chem. Soc.*, 2020, **142**, 3696–3700.

48 S. Clair and D. G. de Oteyza, Controlling a Chemical Coupling Reaction on a Surface: Tools and Strategies for On-Surface Synthesis, *Chem. Rev.*, 2019, **119**, 4717–4776.

49 J. Burroughes, D. Bradley, A. Brown, R. Marks, K. Mackay, R. Friend, P. Burns and A. Holmes, Light-emitting diodes based on conjugated polymers, *Nature*, 1990, **347**, 539–541.

50 D. Baigent, F. Cacialli, N. Greenham, J. Grünner, H. Wittmann, R. Friend, S. Moratti and A. Holmes, Light-emitting diodes fabricated with conjugated polymers, *Solid-State Electron.*, 1996, **40**, 477–485.

51 I. Piquero-Zulaica, A. Garcia-Lekue, L. Colazzo, C. K. Krug, M. S. Mohammed, Z. Abd-El-Fattah, J. M. Gottfried, D. G. de Oteyza, J. E. Ortega and J. Lobo-Checa, Electronic Structure Tunability by Periodic meta-Ligand Spacing in One-Dimensional Organic Semiconductors, *ACS Nano*, 2018, **12**, 10537–10544.

52 A. Basagni, G. Vasseur, C. A. Pignedoli, M. Vilas-Varela, D. Peña, L. Nicolas, L. Vitali, J. Lobo-Checa, D. G. de Oteyza, F. Sedona, M. Casarin, E. Ortega and M. Sambi, Tunable Band Alignment with Unperturbed Carrier Mobility of On-Surface Synthesized Organic Semiconducting Wires, *ACS Nano*, 2016, **10**, 2644–2651.

53 A. Kraft, A. C. Grimsdale and A. B. Holmes, Electroluminescent Conjugated Polymers–Seeing Polymers in a New Light, *Angew. Chem., Int. Ed.*, 1998, **37**, 402–428.

54 L. Dong, P. Liu and N. Lin, Surface-Activated Coupling Reactions Confined on a Surface, *Acc. Chem. Res.*, 2015, **48**, 2765–2774.

55 M. D. Giovannantonio, M. Tomellini, J. Lipton-Duffin, G. Galeotti, M. Ebrahimi, A. Cossaro, A. Verdini, N. Kharche, V. Meunier, G. Vasseur, Y. Fagot-Revurat, D. Perepichka, F. Rosei and G. Contini, Mechanistic Picture and Kinetic Analysis of Surface-Confined Ullmann Polymerization, *J. Am. Chem. Soc.*, 2016, **138**, 16696–16702.

56 M. D. Giovannantonio, M. El-Garah, J. Lipton-Duffin, V. Meunier, L. Cardenas, Y. Fagot-Revurat, A. Cossaro, A. Verdini, D. Perepichka, F. Rosei and G. Contini, Insight into Organometallic Intermediate and Its Evolution to Covalent Bonding in Surface-Confined Ullmann Polymerization, *ACS Nano*, 2013, **7**, 8190–8198.

57 L. Patera, J. Amber and J. Repp, On-Surface Synthesis of Polypyridine: Strain Enforces Extended Linear Chains, *Chemistry*, 2022, **4**, 112–117.

58 S. Howard, Conformers, Energetics, and Basicity of 2,2′-Bipyridine, *J. Am. Chem. Soc.*, 1996, **118**, 10269–10274.

59 J. Xu, S. Xing, J. Hu and Z. Shi, Stepwise on-surface synthesis of nitrogen-doped porous carbon nanoribbons, *Commun. Chem.*, 2024, **7**, 40.

60 X. Shuaipeng, Z. Zhang, X. Fei, W. Zhao, R. Zhang, T. Lin, D. Zhao, H. Ju, H. Xu, J. Fan, J. Zhu, Y. Ma and Z. Shi, Selective on-surface cobalent coupling based on metal-organic coordination template, *Nat. Commun.*, 2019, **10**, 70.

61 X. Zhang, N. Xue, C. Li, N. Li, H. Wang, N. Kocić, S. Beniwal, K. Palotás, R. Li, Q. Xue, S. Maier, S. Hou and Y. Wang, Coordination-Controlled C–C Coupling Products via *ortho*-Site C–H Activation, *ACS Nano*, 2019, **13**, 1385–1393.

62 H. Liang, S. Xing, Z. Shi, H. Zhang and L. Chi, Directing On-Surface Reaction Pathways via Metal-Organic Cu–N Coordination, *ChemPhysChem*, 2020, **21**, 843–846.

63 N. Merino-Díez, A. Garcia-Lekue, E. Carbonell-Sanromà, J. Li, M. Corso, L. Colazzo, F. Sedona, D. Sánchez-Portal, J. I. Pascual and D. G. de Oteyza, Width-Dependent Band Gap in Armchair Graphene Nanoribbons Reveals Fermi Level Pinning on Au(111), *ACS Nano*, 2017, **11**, 11661–11668.

64 C. Bronner, S. Stremlau, M. Gille, F. Braußе, A. Haase, S. Hecht and P. Tegeder, Aligning the Band Gap of Graphene Nanoribbons by Monomer Doping, *Angew. Chem., Int. Ed.*, 2013, **52**, 4422–4425.

65 J. Cai, C. A. Pignedoli, L. Talirz, P. Ruffieux, H. Söde, L. Liang, V. Meunier, R. Berger, R. Li, X. Feng, K. Müllen and R. Fasel, Graphene nanoribbon heterojunctions, *Nat. Nanotechnol.*, 2014, **9**, 896–900.
66 Q. Fan, J. Dai, T. Wang, J. Kuttner, G. Hilt, M. Gottfried and J. Zhu, Confined Synthesis of Organometallic Chains and Macrocycles by Cu-O Surface Templating, *ACS Nano*, 2011, **16**, 3747–3754.
67 S. Wang and W. W. N. Lin, Resolving Band-Structure Evolution and Defect-Induced States of Single Conjugated Oligomers by Scanning Tunneling Microscopy and Tight-Binding Calculations., *Phys. Rev. Lett.*, 2011, **106**, 206803.
68 N. Merino-Díez, J. Lobo-Checa, P. Nita, A. Garcia-Lekue, A. Basagni, G. Vasseur, F. Tiso, F. Sedona, P. K. Das, J. Fujii, I. Vobornik, M. Sambi, J. I. Pascual, J. E. Ortega and D. G. de Oteyza, Switching from Reactant to Substrate Engineering in the Selective Synthesis of Graphene Nanoribbons, *J. Phys. Chem. Lett.*, 2018, **9**, 2510–2517.
69 D. Nečas and P. Klapetek, Gwyddion: an open-source software for SPM data analysis, *Open Phys.*, 2012, **10**, 181.